Hindawi
Journal of Nanomaterials
Volume 2020, Article ID 7147130, 11 pages
https://doi.org/10.1155/2020/7147130

Research Article

In Vitro Cytotoxicity and Antitumor Activity of Dual-Targeting Drug Delivery System Based on Modified Magnetic Carbon by Folate

Jinglei Du,[1] Qiang Li,[1] Lin Chen,[2] Shicai Wang,[1] Li Zhang,[3] Shiping Yu,[1,2] Yongzhen Yang,[2] and Xuguang Liu[2]

[1]*Department of Interventional Therapy, The Second Hospital of Shanxi Medical University, Taiyuan 030001, China*
[2]*Key Laboratory of Interface Science and Engineering in Advanced Materials (Taiyuan University of Technology), Ministry of Education, Taiyuan 030024, China*
[3]*Urology Department, Shanxi Dayi Hospital, Taiyuan 030032, China*

Correspondence should be addressed to Shiping Yu; yushiping6@126.com and Yongzhen Yang; yyztyut@126.com

Received 1 October 2019; Revised 19 November 2019; Accepted 27 November 2019; Published 9 January 2020

Academic Editor: Ruibing Wang

A dual-targeting drug delivery system (DTDDS) with magnetic targeting and active targeting was obtained to improve the targeting and drug-loading capacity of magnetic drug nanocarriers. An ultraviolet-visible spectrophotometer and flow cytometry were used to investigate the drug-loading and release capacity, cytotoxicity, and inhibition of tumor cell proliferation, separately. Results show that DTDDS has obvious magnetic characteristics, on which the modification amount of folic acid is 64.82 mg g^{-1}. Doxorubicin was taken as a template drug to evaluate its drug-loading capacity, which was as high as 577.12 mg g^{-1}. Good biocompatibility and low cytotoxicity of DTDDS were further confirmed. Moreover, DTDDS can target the folate receptor on the surface of HeLa cells and deliver doxorubicin into HeLa cells, thereby increasing the proliferation inhibition for cancer cells. Therefore, this new dual-targeting drug delivery system shows potential in significantly reducing the toxic side effects of chemotherapy and improving chemotherapy efficiency.

1. Introduction

For nearly half a century, malignant tumors have become a major killer of human health. At present, the main methods for treating tumors include surgical resection, chemotherapy, and radiotherapy [1]. Among them, the chemotherapy method using chemical drugs to inhibit tumor cells has become the main means of tumor treatment because of their small traumaticity. However, the biggest disadvantage of traditional chemotherapeutic drugs used in clinical practice is their lack of tissue selectivity. Conventional therapeutic doses have significant toxic side effects on normal tissues and organs, which is why the amount of drugs actually entering the tumor cells is limited. This not only affects the therapeutic effect of the tumor but also destroys the immune system and finally causes gastrointestinal reactions, bone marrow suppression, etc. [2]. Therefore, nanodrug delivery systems with high efficiency of drug utilization and low toxic side effects have become hot issues in current chemotherapy research [3].

Magnetic nanoparticles are widely used in drug carriers because of their unique magnetic responsiveness, good biocompatibility, and low toxicity [4]. They can also be targeted to lesion sites under the action of an external magnetic field and reduce the systemic distribution of cytotoxic drugs, thereby reducing side effects and dosage. However, further studies have found that magnetic targeting drug delivery systems have a poor ability of entering into cancerous cells, although they can be localized in the intercellular substance of cancerous cells, resulting in their low therapeutic efficiency [5]. Delightedly, active targeting provides a new idea for solving this disadvantage [6]. Active targeting can be achieved by modifying the specific ligand on the surface of the drug carrier, which can be actively linked to the receptor on the

surface of the tumor cell. It can avoid being uptaken by the macrophage and can improve the affinity between the drug carrier and the tumor cell, thereby improving the targeting efficiency of the drug carrier. Folate receptors are highly expressed on the surface of various tumor cells, while they are rarely expressed on the surface of normal cells, which provides a new opportunity for targeted treatment of tumors [7]. Therefore, combining magnetic targeting and folate active targeting and synthesizing a dual-targeting nanodrug-controlled release system will show higher targeting efficiency and therapeutic effect on the tumor.

As a new inorganic nanomaterial with high specific surface area, large pore volume, good biocompatibility, and high drug loading, ordered mesoporous carbon nanomaterials have become an ideal drug delivery carrier. It shows great potential in the treatment of malignant tumors with high efficacy [8, 9].

For the design of a novel drug delivery system, the evaluation of biocompatibility, cytotoxicity, and proliferation inhibition for cancer cells is fundamental and necessary [10] Generally, healthy human blood, normal cells, and tumor cells need to be taken as research objects to investigate the biocompatibility of the dual-targeting drug delivery system (DTDDS) by means of hemolysis and flow cytometry. Herein, in order to improve the targeting performance and drug-loading capacity of magnetic nanodrug carriers, DTDDS, which was obtained by using magnetic ordered mesoporous carbon nanospheres as a magnetic targeting drug carrier matrix followed by their modification by folate with active targeting, was applied to investigate the drug-loading and release capacity, biocompatibility (including blood compatibility and histocompatibility), cytotoxicity, and inhibition of tumor cell proliferation. These investigations provide a new method for the targeted treatment of tumors in vivo and lay a theoretical basis for clinical application.

2. Experiments

2.1. Materials. 1-(3-Dimethylaminopropyl)-3-ethylcarbodiimide hydrochloride (EDC, 97%) and N-hydroxysuccinimide (NHS, 98%) were purchased from Beijing J&K Scientific Ltd. Folate (97%) was purchased from Maya Reagent Co., Ltd. Anhydrous ethanol (C_2H_5OH, 99.7%), N-(β-aminoethyl)-γ-aminopropyltrimethoxysilane coupling agent (KH-792), glacial acetic acid (CH_3COOH, 99.5%), and glutaraldehyde were all obtained from Tianjin Guangfu Technology Development Co., Ltd. Doxorubicin (DOX) and 4-hydrazinobenzoic acid (HBA, 98%) were supplied by Shanghai MackLin Biochemical Co., Ltd. Trypsin-EDTA digestive solution (0.25%), DMEM high-sugar medium, and fetal bovine serum were provided by Wuhan Bude Bioengineering Co., Ltd. Cell Counting Kit-8 Kit (CCK-8), Hoechst 33258, and Annexin V-FITC/PI Kit were purchased from Shanghai Biyuntian Biotechnology Co., Ltd. All reagents were of analytical grade.

2.2. Synthesis of DTDDS. Magnetically ordered mesoporous nanoparticles were prepared as previously reported by Chen et al. [11]. To graft folate on its surface, the amino and hydrazine groups were firstly introduced to obtain hydrazine-grafted magnetic ordered mesoporous nanoparticles [12, 13]. As these nanoparticles only show a magnetic targeting effect, they were named magnetic targeting drug delivery system (MTDDS) in this work. Then, their modification by folate was carried out by the activation of the carboxyl group. Three milligrams of EDC and 3 mg of NHS were added into 10 mL of folate solution (800 $\mu g\,mL^{-1}$) for ultrasonic dispersion for 30 min, and then 4 mg of MTDDS was suspended in the above solution and continued to react for 24 h at 25°C. After the reaction was completed, it was separated and purified to obtain DTDDS. Finally, a certain amount of DTDDS was dissolved in 10 mL of PBS solution, and the modification amount of folate was calculated according to the UV-vis absorbance of folate at 350 nm in combination with the standard curve of folate.

2.3. DOX Loading Performance. Loading of DOX molecules was achieved by chemical and physical adsorption of DTDDS [12, 14]. Firstly, DTDDS powder is quantitatively added to a PBS solution (pH = 7.4) and ultrasonically dispersed to obtain different concentrations (100, 200, 300, 500, 800, and 1000 $\mu g\,mL^{-1}$) of a DOX solution. They were placed in a constant-temperature shaker and subjected to a light-proof drug-loading experiment at room temperature and 160 rpm. The solution was magnetically separated and lyophilized to obtain DTDDS@DOX. Finally, the upper layer solution was collected and the absorbance of DOX was measured by UV-vis. The drug-loading amount of DOX at equilibrium was calculated according to the DOX standard curve and equation (1) [15]:

$$Q_e = \frac{(C_0 - C_e) \times V}{M}, \quad (1)$$

where C_0 ($\mu g\,mL^{-1}$) is the initial DOX concentration, C_e ($\mu g\,mL^{-1}$) is the equilibrium DOX concentration, V (mL) is the volume of DOX solution, and M (mg) is the weight of DTDDS. To confirm the targeting effects of DTDDS@DOX, the DOX loading on MTDDS was also conducted on the same condition to obtain (MTDDS@DOX).

2.4. DOX Release Performance In Vitro. According to the drug-loading results, DTDDS with the maximum equilibrium drug-loading capacity (577.12 $mg\,g^{-1}$) was used to evaluate the release properties. Four milligrams of DTDDS@DOX was dispersed in 5 mL of PBS buffer solution (pH = 7.4) in a dialysis bag (with a molecular weight of 1000 D), and then the dialysis bag was placed in 50 mL of PBS buffer solution at pH = 5.6 for the release of DOX at 37°C in a constant-temperature shaker (160 rpm). At regular intervals, the quantitative solutions were removed from the beaker for a UV-vis test. At the same time, a quantitative amount of PBS solution was supplemented to the beaker. The absorbance of DOX was measured to calculate the cumulative release rate Q (%) of DOX according to [16]

$$Q(\%) = \frac{V_0 \times C_t + V \times \sum_{n=1}^{r-1} C}{M \times X} \times 100\%, \quad (2)$$

where V_0 (mL) and V (mL) are the total volume of PBS (i.e., 50 mL) and the removed volume of the sample from the release medium at each interval (i.e., 2 mL), C_t (μg mL^{-1}) is the drug concentration at time "t" in the release mediator, M (mg) is the weight of the drug carrier DTDDS@DOX, and X is the drug-loading rate (%) (drug - loading rate (%) = the weight of loaded drug molecules on carrier/the weight of carrier and the drug to be loaded × 100%).

2.5. Biocompatibility of DTDDS with Blood. Once a drug delivery system enters the body by oral or intravenous injection, it will encounter blood and come in contact with it [17]. Hemoglobin release from red blood cells may be caused by the destruction of the erythrocyte membrane. Therefore, it is necessary to investigate the hemolysis analysis by testing the blood compatibility of nanomaterials. The hemolysis rate was calculated, and the biocompatibility of the nanodrug carrier was investigated.

Two milliliters of fresh anticoagulated healthy human blood was added to the centrifuge tube and then diluted with 2.5 mL of 0.9% physiological saline. The diluted fresh healthy human blood was gently mixed for experimental use. The lyophilized DTDDS powder was mixed with 0.9% physiological saline to prepare different concentrations (0.1, 0.3, and 0.5 mg mL^{-1}) of the nanoparticle solution, and each group was repeated in parallel for three times. The distilled water was used as a positive control, and 0.9% physiological saline was set as a negative control, each of which was added to a 15 mL centrifuge tube in an equal volume. The prepared centrifuge tubes of different concentrations of DTDDS solution, physiological saline, and distilled water were placed in a 37°C water bath. After 60 min, 0.3 mL of diluted healthy human blood was completely dispersed in each centrifuge tube and kept in a 37°C water bath for 60 min. Finally, the centrifuge tubes were centrifuged at 2000 rpm min^{-1} for 10 min. After centrifugation, the supernatant was pipetted into a cuvette and measured on a UV-vis. The absorbance (OD) of the supernatant of each group at 545 nm was measured to calculate the hemolysis rate according to [18]

$$\text{Hemolysis rate}\,(\%) = \left(\frac{\text{OD}_{\text{test sample}} - \text{OD}_{\text{negative control}}}{\text{OD}_{\text{positive control}} - \text{OD}_{\text{negative control}}}\right) \times 100\%. \quad (3)$$

The above experiment was repeated 3 times independently. If the hemolysis rate is <5%, the nanocarrier conforms to the requirements of the hemolysis experiment. If the hemolysis rate is >5%, the nanocarrier material has hemolytic toxicity [19].

2.6. Cytotoxicity of Drug Carriers. Cell viability was measured by flow cytometry. HeLa cells were cultured as described above and counted on a hemocytometer plate. They were seeded in a 24-well plate which was previously irradiated with ultraviolet light at a density of 1×10^5/mL per well, and then 1 mL of a single-cell suspension was added to each well. The inoculated 24-well plate was placed in a constant-temperature cell incubator for 24 h to allow the cells to adhere well to the wall. After the cells are attached, the old culture solution is aspirated, washed 3 times with PBS, and then added with different concentrations (0, 25, 50, 75, 100, and 200 μg mL^{-1}) of DTDDS solution and allowed to culture continuously for 24 h. The culture solution and the excess DTDDS were aspirated and washed 3 times with PBS solution. After having been digested with 0.25% trypsin, the cells were washed 3 times with PBS solution, centrifuged at 2000 rpm for 5 min, and collected and mixed by blowing. The supernatant were discarded and the cells were resuspended by adding 500 μL of binding buffer. After adding 5 μL of Annexin V-FITC, 5 μL of PI were mixed with the cells and protected from light for 10-15 min.

2.7. Proliferation Inhibition for HeLa Cells. In this experiment, the HeLa cells were used to evaluate the proliferation inhibition effect of DOX or DTDDS@DOX (MTDDS@DOX) by the Cell Counting Kit-8 (CCK-8) method. HeLa cells were seeded in a UV-irradiated 96-well plate at a density of 7×10^4/mL per well, and 100 μL of a single-cell suspension was added to each well. The inoculated 96-well plate was placed in a cell culture incubator for 24 h to allow the cells to adhere well to the wall. The DTDDS was suspended in fresh medium and filtered through a 0.22 μm filter. The concentration of DOX, MTDDS@DOX, and DTDDS@DOX were separately arranged as 8, 4, 2, 1, 0.5, 0.25, 0.125, and 0 μg mL^{-1}, and the concentration of 0 μg mL^{-1} was used as a control group. The nonadherent cells of each well were aspirated and washed 3 times with PBS. 100 μL of different concentrations of MTDDS@DOX or DTDDS@DOX solution were added to each well and 5 subwells were set in each group. Subsequently, the 96-well plates were placed in a constant-temperature cell incubator for 24 and 48 h, respectively. Then, the 96-well plate was taken out. The supernatant was aspirated and washed 2-3 times with PBS. 100 μL of fresh medium was added. Finally, 10 μL of the CCK-8 reagent was added to each well and allowed to incubate continuously for 4 h in the dark. The OD value at 450 nm of each well was measured with a microplate reader. The relative survival rate of the cells = $(\text{OD}_{\text{experimental group}}/\text{OD}_{\text{control group}}) \times 100\%$. The above experiment was repeated 3 times independently.

Moreover, the morphology of the HeLa cells was also investigated to further confirm their effect of proliferation inhibition. HeLa cells were seeded on a pre-UV-irradiated 6-well plate at a density of 5×10^4 cells/mL per well, and 2 mL of a single-cell suspension was added to each well. The inoculated 6-well plate was placed in a cell culture incubator for 24 h to allow the cells to adhere. Then, DOX, MTDDS@DOX, and DTDDS@DOX solutions were added separately and allowed to culture continuously for 6 and 12 h. The fresh medium was set as the blank control group. The growth of each group of cells was observed by an inverted microscope.

2.8. Intracellular Uptake of DOX by HeLa Cells. Hoechst 33258 is a blue fluorescent dye that can penetrate cell membranes. It can be specifically bonded to double-stranded DNA and shows nuclear morphology. It is less toxic to cells and is suitable for most cell staining. At the same time,

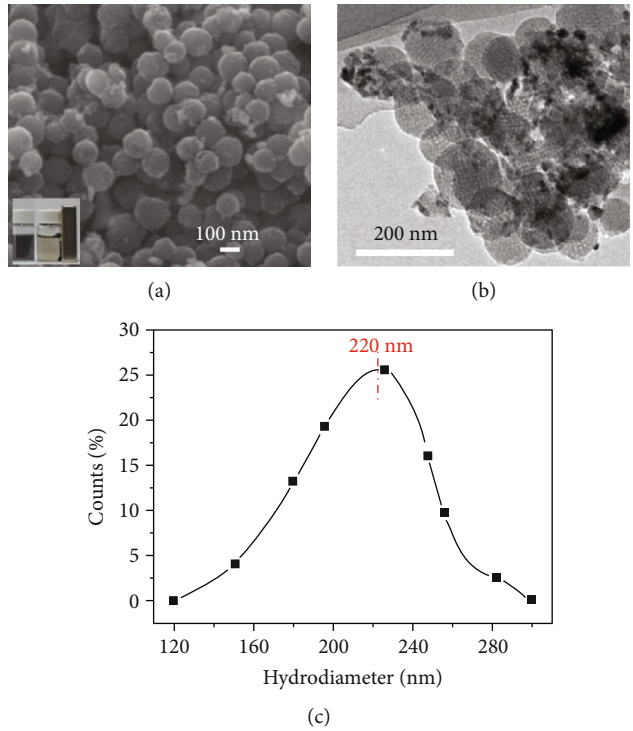

Figure 1: (a) FESEM and (b) TEM images and (c) size distribution of DTDDS; inset is the photograph of magnetic separation for DTDDS dispersion.

DOX has intrinsic red fluorescence; therefore, the combination of Hoechst 33258 and DOX can be used to observe the uptake and distribution of DOX in cells. In this study, HeLa cells were used as effector cells, and the uptake ability of HeLa cells to three drugs (DOX, MTDDS@DOX, and DTDDS@DOX) was qualitatively observed by an inverted fluorescence microscope. The concentrations of the drugs were compared at the same concentrations, and the fluorescence intensity of DOX in the cell was observed to verify the tumor targeting of the drug carrier modified by folate.

DOX, MTDDS@DOX, and DTDDS@DOX were dispersed in fresh medium, filtered through a 0.22 μm filter, and diluted. HeLa cells were cultured on a 6-well plate at a density of 5×10^4 cells/mL per well. When the adherent cell growth coverage reached 80% to 90%, the supernatant was removed and washed with PBS for 3 times. Each plate was divided into three groups, and each group was paralleled two times. The solution of DOX, MTDDS@DOX, or DTDDS@DOX was added into cells separately, and then placed in a cell culture incubator for a further 4 h. Subsequently, the medium of each well was aspirated with a pipette. The remaining nanoparticles in the solution in each well were rinsed with PBS buffer for 10 min $\times$ 3 times. Glutaraldehyde (2.5%) was used to fix the cells for 10 min at 4°C. After being rinsed by PBS buffer, 100 μL of Hoechst 33258 solution was added into each well and kept for 10 min. The staining process should be placed under the microscope to prevent overstaining. To avoid cells from being inactivated for a long time after rinsing, they should be immediately observed and photographed under an inverted fluorescence microscope.

2.9. Instruments. The morphology feature of DTDDS was analyzed by a field emission electron microscope (FESEM, JEOL JSM-6700F, Japan) and a transmission electron microscope (TEM, JEM-100CXII, Japan). The average hydrodynamic diameter of the nanospheres was measured using dynamic light scattering (DLS) of a Zetasizer Nano ZS90 (Malvern Instruments, UK). UV-vis absorption spectra were recorded on a Hitachi U-3900 UV-vis spectrophotometer (Hitachi High-Technologies, Japan). A multifunction microplate reader (BioTek Instruments, CYT3MF, USA) and a flow cytometer were used to detect the viability of cells (Beckman Coulter, FC500, USA). Cellular images were acquired with an inverted microscope (Olympus, Japan).

3. Results and Discussion

3.1. Structure and Dual-Targeting Properties of DTDDS. The morphology of DTDDS was observed by FESEM (Figure 1(a)) and TEM (Figure 1(b)), which shows that they are in a spherical morphology with an ordered mesoporous structure and an average size of about 100 nm. To further characterize their size information, the hydrodynamic diameter of DTDDS was measured in PBS suspension, which is around 220 nm, as shown in Figure 1(c). It is worth mentioning that the size obtained by DLS is about 120 nm higher than that measured by SEM, which can be illustrated by the fact that there exists a hydrated layer around the surfaces of DTDDS as it was measured in the aqueous solution. At the same time, the zeta potential of DTDDS in PBS at a concentration of 80 μg mL^{-1} was obtained, which is -27.0 mV, demonstrating their relative stability in PBS.

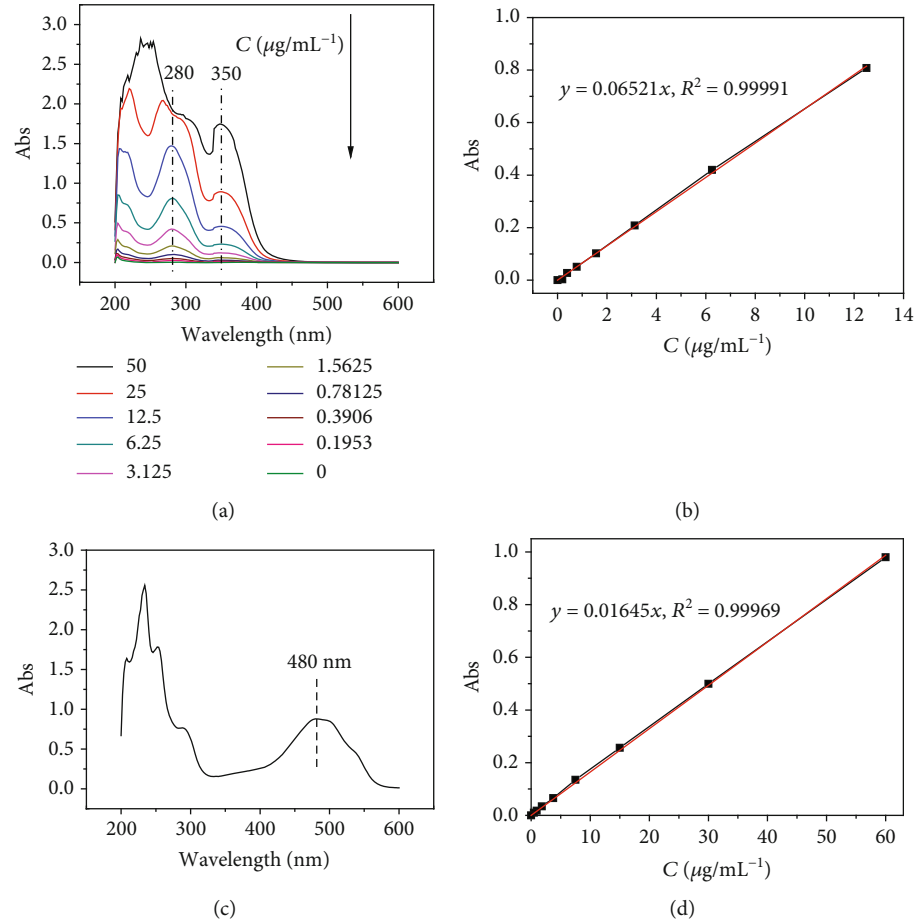

FIGURE 2: UV-vis spectra of folate (a) and standard curve (b). UV-vis spectra of DOX (c) and standard curve (d).

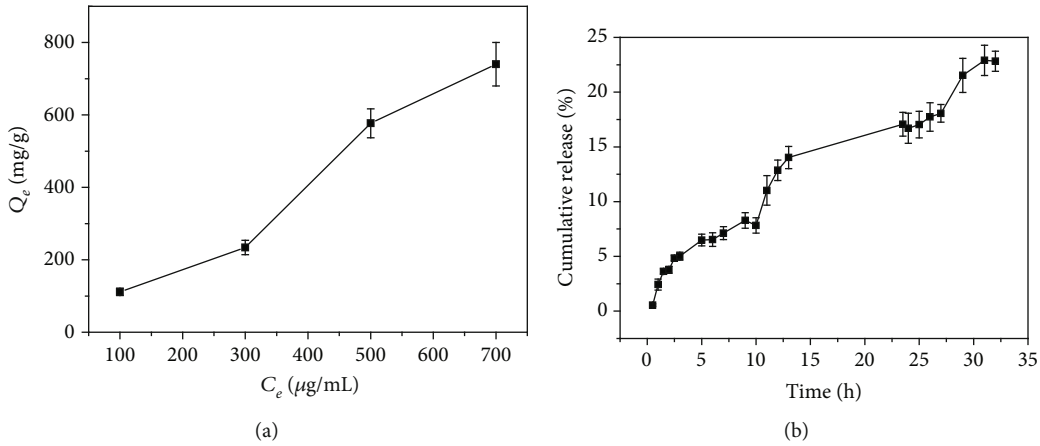

FIGURE 3: (a) DOX loading and (b) release curves at 37°C.

The insert in Figure 1(a) is a picture of DTDDS in PBS solution before and after magnetic separation. It can be seen that DTDDS moves towards the magnet and finally gathers on the side of the bottle when a magnet of 0.24 T is close to the aqueous dispersion, proving that DTDDS has potential in the magnetic targeting area.

The folate grafting amount onto DTDDS was calculated by the standard curve. Figure 2(a) shows the UV-vis curves of different concentrations of folate solution. It can be seen that the characteristic absorption peaks of folate are at 280 and 350 nm. At low concentrations, the absorbance and concentrations of folate at 280 nm are more consistent in a linear relationship. Therefore, 280 nm was chosen as the characteristic absorption peak of folate. The relationship of Abs-C can be obtained by linear regression, as shown in Figure 2(b). In the range of 0-15 $\mu g\,mL^{-1}$, the

standard curve equation is $y = 0.06521x$, $R^2 = 0.99991$. Combined with the standard curve of folate, the average modification amount of folate by DTDDS is 64.82 mg g^{-1}. As reported, the grafting amount of folate around this value could achieve active targeting [15]. These results demonstrate that DTDDS has the ability of dual-targeting including magnetic and active targeting because of its magnetism and folic acid components.

3.2. DOX Loading and Release Properties of DTDDS. The drug-loading capacity and release properties of DTDDS can remarkably affect its efficacy of cancer therapy. Therefore, the effect of DOX concentration on the drug loading of DTDDS and the performance of release in vitro were evaluated. First of all, the UV-vis spectrum of DOX was measured from 200 to 600 nm. The characteristic absorptions are located at 232 and 480 nm, as shown in Figure 2(c), and the absorbance value at 480 nm has a linear relationship with the concentration. Therefore, it is selected as the characteristic absorption peak of DOX in this work. The relationship of Abs-C can be obtained by linear regression, as shown in Figure 2(d). In the range of 0-60 μg mL^{-1}, the standard curve equation is $y = 0.01645x$, $R^2 = 0.99969$.

The DOX loading results are shown in Figure 3. According to Figure 3(a), the loading amount of DOX increases with the change of its initial concentration and up to 577.12 mg g^{-1} at the concentration of DOX of 500 μg mL^{-1}. It is expected that the drug loading will continue to increase with the increase of DOX concentration. The drug-loading mechanism of DOX on DTDDS can be attributed to an integration of monolayer and multilayer adsorption, as both porous adsorption and covalent interactions take place during the drug-loading process [11]. Therefore, the loading rate is affected by the concentration of DOX, the diffusion rate of DOX in PBS, and also the interactions between DOX and DTDDS. In Figure 3(a), with the increase of the concentration of DOX, the loading rate initially increases and then decreases. It can be inferred that when the concentration is quite low or high, porous adsorption dominates in the loading, which is a little slow. While when the concentration increases to 300 and 500 μg mL^{-1}, covalent interactions dominate, leading to a much higher loading rate.

As shown in Figure 3(b), the release profile of DOX in DTDDS was carried out at 37°C when the pH is 5.6 due to the lower pH value inside the cancer cell. From the release curve, it can be intuitively found that the release rate can reach more than 20% in 30 h of release time, demonstrating its good controlled release. As mentioned before [11], the high drug loading of DTDDS obtained in this work can be attributed to the combination of physical and chemical forces, indicating that the force between DOX and DTDDS is relatively strong, which is also an important reason for its slow release.

3.3. Biocompatibility of DTDDS with Blood. Fresh anticoagulated healthy human blood was used to study the hemolysis rate of DTDDS, in which saline was set up as a negative control and distilled water was set as a positive control. The hemolysis rate of DTDDS was calculated to verify its blood compatibility. The experimental results are shown in Table 1 and Figure 4. The hemolysis rate of each group of DTDDS is less than 5%. Compared with the positive control group, the P value is less than 0.05 and the difference is significant. There is no difference compared with the negative control group. Therefore, DTDDS meets the requirements for the hemolysis rate of medical materials.

Table 1: Hemolysis rate of DTDDS ($n = 3$, $\bar{\chi} \pm S$).

Samples	Concentration (mg mL^{-1})	Mean OD value	Hemolysis rate (%)	P value
DTDDS	0.100	0.013 ± 0.002	1.0	0.006
	0.300	0.019 ± 0.002	1.5	0.007
	0.500	0.024 ± 0.002	2.0	0.007
Saline		0.003 ± 0.001	0.0	
Distilled water		1.041 ± 0.061	100	

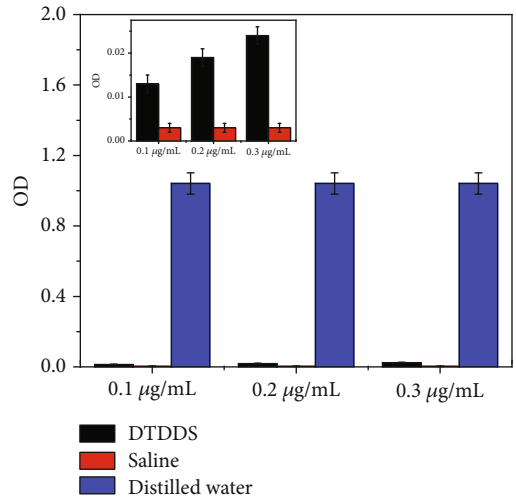

Figure 4: Hemolysis analysis of DTDDS.

Table 2: Cell viability of different concentrations of DTDDS against HeLa cells detected by flow cytometry ($n = 5$, $\bar{\chi} \pm S$).

Concentration (μg mL^{-1})	Cell viability (%)	t value	P value
200	64.70 ± 1.47	35.106	<0.05
100	76.05 ± 1.29	23.2	<0.05
75	79.46 ± 1.09	20.449	<0.05
50	80.56 ± 1.05	19.192	<0.05
25	92.69 ± 1.34	1.758	0.117
0	93.79 ± 1.13		

3.4. Cytotoxicity of DTDDS. The determination of cell viability of DTDDS is critical when evaluating its response to cytotoxic drugs or other environmental factors. Recently, flow cytometry provides a rapid and reliable method to

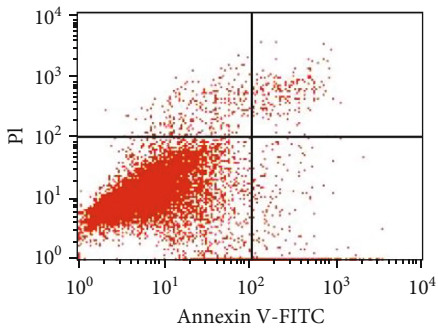

Quad	Events	% gated
UL	293	1.78
UR	192	1.17
LL	15422	93.92
LR	514	3.13

(a)

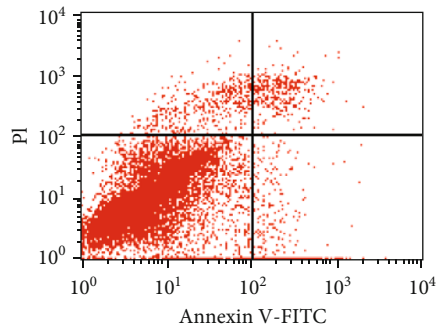

Quad	Events	% gated
UL	459	2.55
UR	355	1.97
LL	16640	92.30
LR	574	3.18

(b)

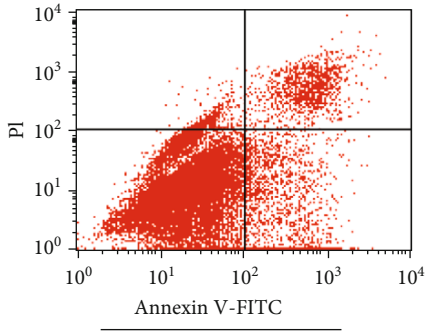

Quad	Events	% gated
UL	468	2.56
UR	1227	6.70
LL	14706	80.35
LR	1901	10.39

(c)

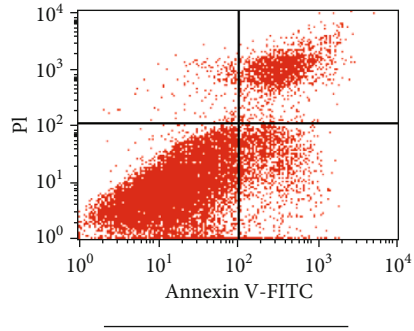

Quad	Events	% gated
UL	194	1.13
UR	1849	10.74
LL	13683	79.46
LR	1494	8.68

(d)

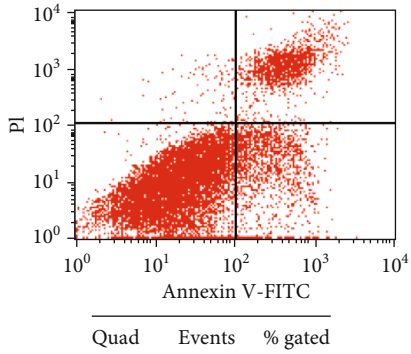

Quad	Events	% gated
UL	102	0.79
UR	1450	11.21
LL	9892	76.45
LR	1495	11.55

(e)

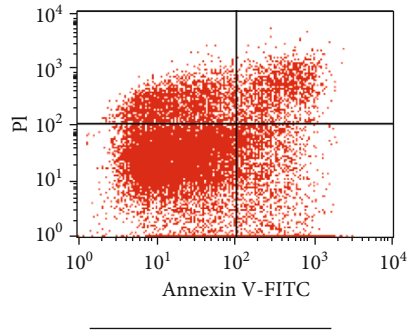

Quad	Events	% gated
UL	2393	12.70
UR	1422	7.55
LL	12386	65.74
LR	2639	14.01

(f)

Figure 5: Cell viability of DTDDS against HeLa cells with different carrier concentrations measured by flow cytometry: (a) 0 μg mL^{-1}, (b) 25 μg mL^{-1}, (c) 50 μg mL^{-1}, (d) 75 μg mL^{-1}, (e) 100 μg mL^{-1}, and (f) 200 μg mL^{-1}.

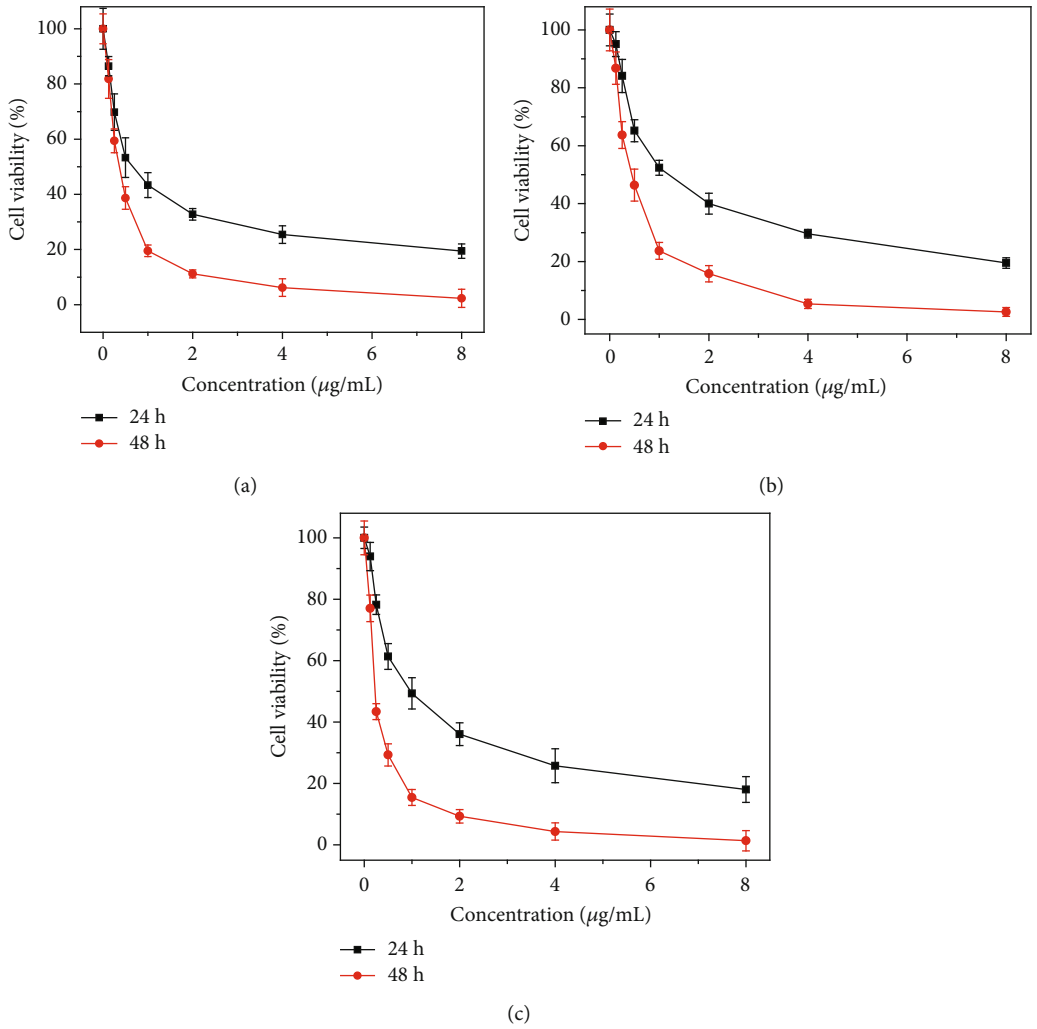

Figure 6: Cell viability of HeLa cells after coincubation with series concentrations of DOX (a), MTDDS@DOX (b), and DTDDS@DOX (c) for 24 and 48 h.

quantify viable cells in a cell suspension. Propidium iodide (PI) is a membrane impermeant dye that is generally excluded from viable cells. PI is excited at 488 nm with a relatively large Stokes shift and emits at a maximum wavelength of 617 nm. Because of these spectral characteristics, the cell viability is obtained by counting the percentage of viable cells in all cells. To further verify the biosafety of the drug carrier, flow cytometry-Annexin V/PI double staining was used to detect the cell viability of different concentrations of DTDDS against HeLa cells after incubation for 24 h. The experimental results are shown in Table 2 and Figure 5. The concentrations of DTDDS in the groups of 50, 75, 100, and 200 $\mu g\,mL^{-1}$ are significantly different from those in the control group ($P < 0.05$). When the concentration of DTDDS is 100 $\mu g\,mL^{-1}$, the cell viability reaches 76.05 ± 1.29%. In Figure 5, UR represents late apoptotic rate, LR represents early cell apoptosis rate, UL represents cell death rate, and LL represents cell survival rate. The results verified the biosafety of DTDDS. Therefore, the cytotoxicity produced by the drug carrier DTDDS in the subsequent experiments can be negligible.

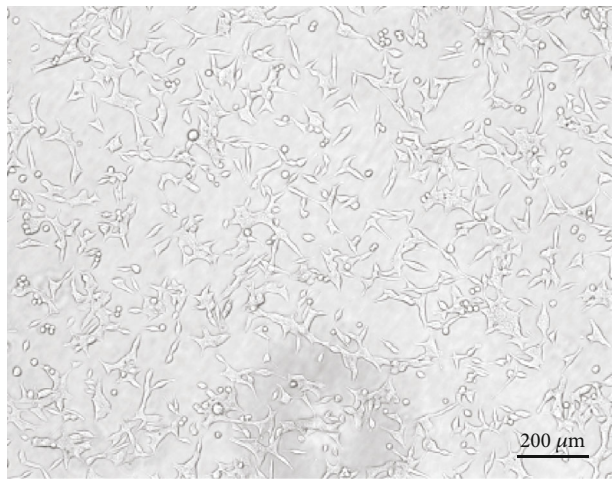

Figure 7: Optical micrographs of HeLa cells.

3.5. Proliferation Inhibition for HeLa Cells. To confirm the therapeutic efficiency of DTDDS as an intracellular nanocarrier, free DOX, MTDDS@DOX, and DTDDS@DOX were

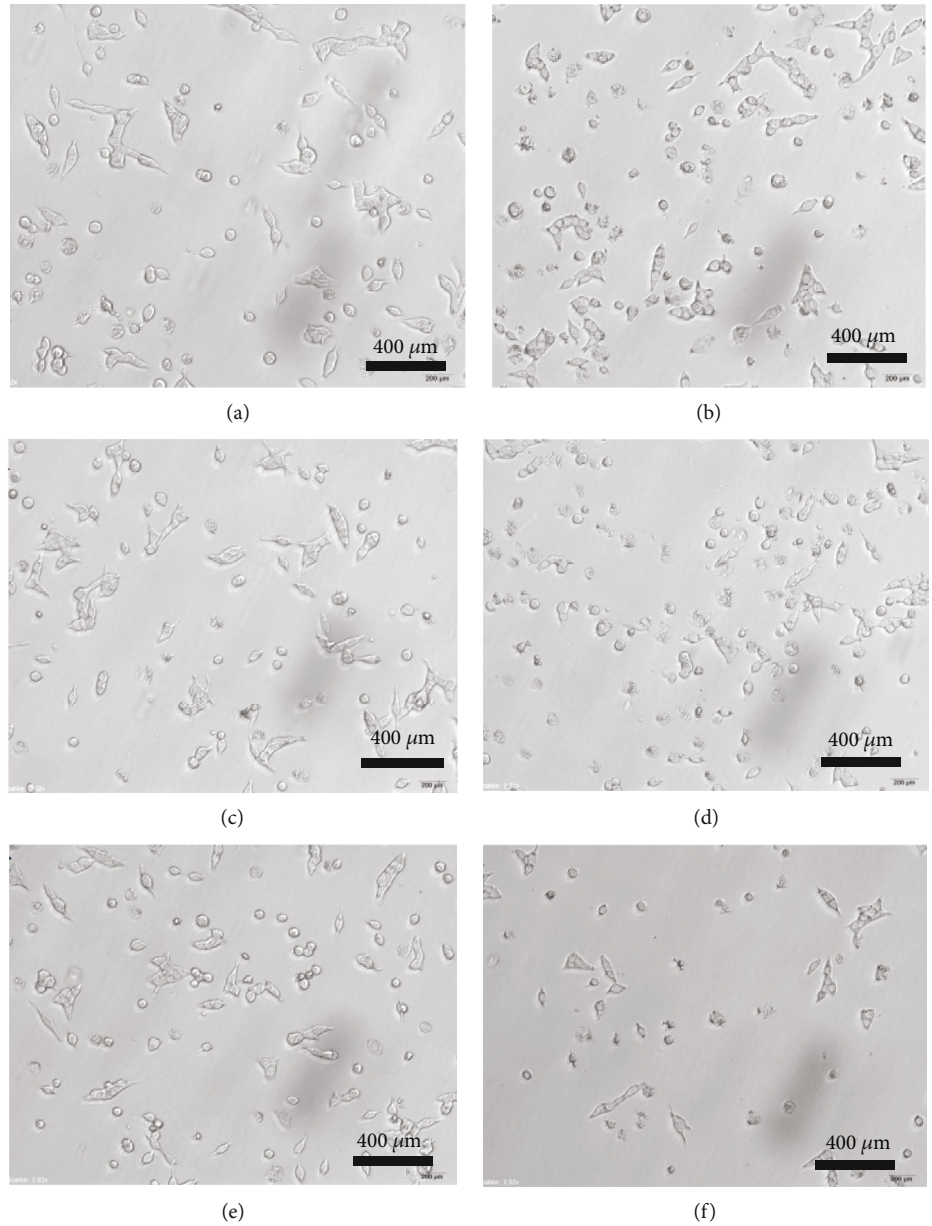

Figure 8: Optical micrographs of HeLa cells incubated with free DOX for 6 h (a) and 12 h (b), with MTDDS@DOX for 6 h (c) and 12 h (d), and with DTDDS@DOX for 6 h (e) and 12 h (f).

incubated with HeLa cells, and the cell viability was tested by the CCK-8 method. The results are shown in Figure 6. The proliferation inhibition effects of DOX, MTDDS@DOX, and DTDDS@DOX drugs on HeLa cells depend on incubation time and their concentration. With the increase of incubation time and drug concentration, the cell viability decreases gradually. When the drug concentration is less than $1\,\mu g\,mL^{-1}$ and the drug group acts on HeLa cells for 24 h, the proliferation inhibition of the DOX group on HeLa cells is stronger than that of the MTDDS@DOX and DTDDS@DOX groups. When the drug concentration is $1\,\mu g\,mL^{-1}$ and the drug group acts on HeLa cells for 48 h, the proliferation inhibition of the DTDDS@DOX group to HeLa cells is stronger than that of the DOX and MTDDS@DOX groups. These indicate that DTDDS@DOX has a sustained release effect and can target the folate receptor on the surface of HeLa cells to improve the inhibition rate. When the drug concentration is higher than $2\,\mu g\,mL^{-1}$, there is no difference in the inhibition of HeLa cell proliferation by the three drug groups.

The effects of DOX, MTDDS@DOX, and DTDDS@DOX on the morphology and quantity of HeLa cells under an inverted microscope were observed to further reveal the inhibitory effect of the drug-loading system on tumor cells. The results show that the cells in the blank control group grow well and the morphology is uniform, as shown in Figure 7. After 6 h of drug treatment, the number of viable cells decreases significantly, the morphology shrinks, and the apoptotic cells increase (Figures 8(a), 8(c), and 8(e)). After 12 h of drug treatment, the number of viable cells of

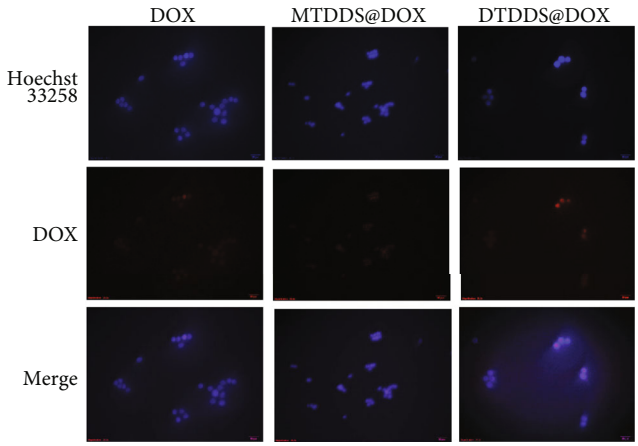

Figure 9: Fluorescence of DOX in HeLa cells.

the DTDDS@DOX group is significantly less than that of the MTDDS@DOX and DOX group (Figures 8(b), 8(d), and 8(f)). There are more cells with morphological shrinkage and apoptosis, and the cell morphology change more obviously, which also indirectly verifies that DTDDS@DOX can target into HeLa cells and has a stronger antitumor effect.

3.6. Intracellular Uptake of DOX by HeLa Cells. To further validate the targeting effect of DTDDS@DOX on HeLa cells, the inverted fluorescence microscopy was used to qualitatively observe the uptake ability of HeLa cells by the pure DOX group, MTDDS@DOX group, and DTDDS@DOX group. The fluorescence intensity of DOX in the cells by the three drug groups at the same drug concentration and the same time was compared. Figure 9 shows the results of fluorescence microscopy after the incubation of DOX, MTDDS@DOX, and DTDDS@DOX on HeLa cells for 4 h, separately. The blue fluorescence is from Hoechst 33258, and the red fluorescence is from DOX. The experimental results show that the intracellular red fluorescence intensity of HeLa cells in the DTDDS@DOX group is significantly stronger than that in the DOX MTDDS@DOX group. This can be attributed to the fact that DTDDS@DOX delivers drugs to cells by targeting folate receptors on the surface of HeLa cells, thereby increasing the intracellular uptake of DOX. Meanwhile, the microenvironment of HeLa cells is weakly acidic, and drug releasing from DTDDS@DOX is easier in a weak acid environment. Therefore, the folate-modified drug-loading system can be used as a highly efficient chemotherapeutic drug carrier to target tumor cells such as HeLa cells that highly express folate receptors, and further enhance the antitumor effect.

4. Conclusions

In summary, the DTDDS with magnetic targeting and active targeting can load 577.12 mg g^{-1} of DOX, and DOX can be released in a controlled manner from DTDDS with a release rate of about 20% in 30 h. The hemolysis rate of DTDDS is less than 5%, which is significantly different from the positive control group and in compliance with the required biocompatibility hemolysis rate. When the concentration of DTDDS is 100 $\mu g\,mL^{-1}$, the cell viability reaches 76.05 ± 1.29%, showing good biocompatibility and low toxicity, which can be used as a highly efficient nanodrug carrier for drug delivery. Because of its good sustained release and targeting properties, DTDDS can more effectively inhibit the proliferation of HeLa cells and reduce the side effects of normal cells. In view of its outstanding performances in drug delivery, DTDDS shows great potential in improving the efficacy of cancer treatment and reducing the side effects.

Data Availability

All data used to support the findings of this study are available from the corresponding author upon request.

Disclosure

Jinglei Du and Qiang Li should be considered as co-first authors.

Conflicts of Interest

The authors declare that they have no conflicts of interest.

Authors' Contributions

Jinglei Du and Qiang Li contributed equally to this work.

Acknowledgments

This work was financially supported by the Natural Science Foundation of Shanxi Province (201901D211502 and 201901D211501), the Shanxi Provincial Excellent Talents Science and Technology Innovation Project (201805D211001), and the National Natural Science Foundation of China (51803148).

References

[1] S. Ahmed and C. Eng, "Role of chemotherapy in the neoadjuvant/adjuvant setting for patients with rectal adenocarcinoma undergoing chemoradiotherapy and surgery or radiotherapy and surgery," *Current Oncology Reports*, vol. 20, no. 1, p. 3, 2018.

[2] J. Tang, R. Zhang, M. Guo et al., "Nucleosome-inspired nanocarrier obtains encapsulation efficiency enhancement and side effects reduction in chemotherapy by using fullerenol assembled with doxorubicin," *Biomaterials*, vol. 167, pp. 205–215, 2018.

[3] R. Ranganathan, S. Madanmohan, A. Kesavan et al., "Nanomedicine: towards development of patient-friendly drug-delivery systems for oncological applications," *International Journal of Nanomedicine*, vol. 7, pp. 1043–1060, 2012.

[4] C. Li, R. Wu, J. Zou et al., "MNPs@anionic MOFs/ERGO with the size selectivity for the electrochemical determination of H_2O_2 released from living cells," *Biosensors and Bioelectronics*, vol. 116, pp. 81–88, 2018.

[5] H. Nosrati, M. Salehiabar, S. Davaran, H. Danafar, and H. K. Manjili, "Methotrexate-conjugated L-lysine coated iron oxide magnetic nanoparticles for inhibition of MCF-7 breast cancer

cells," *Drug Development and Industrial Pharmacy*, vol. 44, no. 6, pp. 886–894, 2018.

[6] D. Rosenblum, N. Joshi, W. Tao, J. M. Karp, and D. Peer, "Progress and challenges towards targeted delivery of cancer therapeutics," *Nature Communications*, vol. 9, no. 1, p. 1410, 2018.

[7] Q. Zhang, F. Liu, K. T. Nguyen et al., "Multifunctional mesoporous silica nanoparticles for cancer-targeted and controlled drug delivery," *Advanced Functional Materials*, vol. 22, no. 24, pp. 5144–5156, 2012.

[8] Y. Kuang, Y. Cao, M. Liu et al., "Geometrical confinement of gadolinium oxide nanoparticles in poly(ethylene glycol)/arginylglycylaspartic acid-modified mesoporous carbon nanospheres as an enhanced T1 magnetic resonance imaging contrast agent," *ACS Applied Materials & Interfaces*, vol. 10, no. 31, pp. 26099–26107, 2018.

[9] H. Wang, X. Li, Z. Ma et al., "Hydrophilic mesoporous carbon nanospheres with high drug-loading efficiency for doxorubicin delivery and cancer therapy," *International Journal of Nanomedicine*, vol. 11, pp. 1793–1806, 2016.

[10] P. Sathishkumar, F. L. Gu, Q. Zhan, T. Palvannan, and A. R. Mohd Yusoff, "Flavonoids mediated "green" nanomaterials: a novel nanomedicine system to treat various diseases—current trends and future perspective," *Materials Letters*, vol. 210, pp. 26–30, 2018.

[11] L. Chen, H. Zhang, J. Zheng et al., "Thermo-sensitively and magnetically ordered mesoporous carbon nanospheres for targeted controlled drug release and hyperthermia application," *Materials Science and Engineering: C*, vol. 84, pp. 21–31, 2018.

[12] S. Kapri, S. Maiti, and S. Bhattacharyya, "Lemon grass derived porous carbon nanospheres functionalized for controlled and targeted drug delivery," *Carbon*, vol. 100, pp. 223–235, 2016.

[13] J. Zhou, G. Romero, E. Rojas, L. Ma, S. Moya, and C. Gao, "Layer by layer chitosan/alginate coatings on poly(lactide-co-glycolide) nanoparticles for antifouling protection and folic acid binding to achieve selective cell targeting," *Journal of Colloid and Interface Science*, vol. 345, no. 2, pp. 241–247, 2010.

[14] Y. Lv, L. Tao, S. W. Annie Bligh, H. Yang, Q. Pan, and L. Zhu, "Targeted delivery and controlled release of doxorubicin into cancer cells using a multifunctional graphene oxide," *Materials Science and Engineering: C*, vol. 59, pp. 652–660, 2016.

[15] D. Huang, Y. Zhuang, H. Shen, F. Yang, X. Wang, and D. Wu, "Acetal-linked PEGylated paclitaxel prodrugs forming free-paclitaxel-loaded pH-responsive micelles with high drug loading capacity and improved drug delivery," *Materials Science and Engineering: C*, vol. 82, pp. 60–68, 2018.

[16] L. Chen, L. Li, H. Zhang et al., "Magnetic thermosensitive core/shell microspheres: synthesis, characterization and performance in hyperthermia and drug delivery," *RSC Advances*, vol. 4, no. 87, pp. 46806–46812, 2014.

[17] H. Nosrati, N. Rashidi, H. Danafar, and H. K. Manjili, "Anticancer activity of tamoxifen loaded tyrosine decorated biocompatible Fe_3O_4 magnetic nanoparticles against breast cancer cell lines," *Journal of Inorganic and Organometallic Polymers and Materials*, vol. 28, no. 3, pp. 1178–1186, 2018.

[18] T. Yu, A. Malugin, and H. Ghandehari, "Impact of silica nanoparticle design on cellular toxicity and hemolytic activity," *ACS Nano*, vol. 5, no. 7, pp. 5717–5728, 2011.

[19] P. Kumari, M. O. Swami, S. K. Nadipalli, S. Myneni, B. Ghosh, and S. Biswas, "Curcumin delivery by poly(lactide)-based copolymeric micelles: an in vitro anticancer study," *Pharmaceutical Research*, vol. 33, no. 4, pp. 826–841, 2016.